Synthesis of High Surface Area Aluminophosphate and -phosphonate Xerogels by Non-Hydrolytic Sol-Gel Reactions

Petr Machac,[a] Johan G. Alauzun,[b] Ales Styskalik,[a,c] Damien P. Debecker,[d] P. Hubert Mutin,[b] and Jiri Pinkas[a,c]*

[a] Masaryk University, Faculty of Science, Department of Chemistry, Kotlarska 2, 61137 Brno, Czech Republic
[b] Institut Charles Gerhardt Montpellier, UMR 5253, CNRS-Université de Montpellier-ENSCM, Montpellier Cedex 5 34095, France
[c] Masaryk University, CEITEC MU, Kamenice 5, 62500 Brno, Czech Republic
[d] Institute of Condensed Matter and Nanoscience (IMCN), UCLouvain, Place Louis Pasteur 1, 1348 Louvain-La-Neuve, Belgium

*Corresponding author.

E-mail address: jpinkas@chemi.muni.cz (JP)

Abstract

We disclose the preparation of high-surface-area mesoporous aluminophosphates and aluminophosphonates by the non-hydrolytic sol-gel reactions (NHSG) of $Al(NMe_2)_3$ with trimethylsilylated phosphate $OP(OSiMe_3)_3$, phosphonates $RP(O)(OSiMe_3)_2$ (R = Me, ^tBu, Ph), and bis-phosphonates $(Me_3SiO)_2(O)P–X–P(O)(OSiMe_3)_2$ (X = C_6H_4, $(C_6H_4)_2$) in dry toluene. The reactions proceed by silylamine elimination of Me_3SiNMe_2 to provide organic-inorganic hybrid xerogels with properties influenced by organic substituents and the Al:P ratio of the precursors. Dried xerogels exhibit large surface areas (up to 1000 $m^2 g^{-1}$) and matrices based on condensed Al–O–P networks. They stay stable under relatively harsh thermal conditions. ^{27}Al, ^{13}C, and ^{29}Si solid-state NMR spectroscopy was employed to characterize the aluminum coordination and the residual amido and trimethylsilyl groups. The catalytic performance of NHSG prepared material was examined in gas-phase dehydration of ethanol to ethylene exhibiting conversion and selectivity comparable to weak solid acid benchmark catalysts. The number of unreacted surface groups was determined by gravimetric measurements and by thermal analysis (TG-DSC). These residual groups have the potential to be used in post-synthetic grafting of catalytically active metal centers.

Keywords

aluminophosphates; aluminophosphonates; non-hydrolytic; sol-gel; silylamine elimination; mesoporous; hybrid; xerogel; surface area; catalysis

1. Introduction

Since the second half of the 20th century, due to the growing importance of petrochemistry and organic synthetic chemistry, one of the main topics of inorganic materials chemistry has been to develop new porous catalysts and sorbents with high surface areas.

Conventional preparations of porous materials by sol-gel or precipitation methods in an aqueous medium usually lead to microporous materials, if no template is present. Non-hydrolytic sol-gel (NHSG) methods introduce a number of novel precursors and allow us to control final properties by varying the nature of building blocks and reaction conditions. Comprehensive reviews of this topic were published recently [1,2]. Organic-inorganic hybrids are attractive materials, which can be synthesized by the NHSG methodology. They combine the inorganic network robustness with properties brought by the organic building blocks, such as controlled hydrophobicity, chemical functionality, and adjustable morphology [3]. Organosilicas are very popular and belong to the most common hybrid materials, but it is known that some applications require conditions incompatible with silica-based materials (e.g., their stability at high pH is limited) [4]. Aluminum phosphates and phosphonates can be used to substitute silica since they can be prepared with similar morphology. Microporous crystalline aluminophosphates (AlPO-n) have been intensively studied for their porosity and Brønsted acidic sites (P–OH), which entail on them catalytic activity [5]. Nowadays, the research is focused on the incorporation of catalytically active centers (usually transition metals, such as Rh, Pd, Fe, Co, etc.) into the AlPO matrices [6–8]. Easily prepared and well-defined supports for such catalysts are crucial as many technical demands are placed on these materials. The most relevant parameters are a high surface area (SA) and pore size in the mesoscale range. Mesoporous materials allow for attaining high catalytic efficiencies even with low loadings of transition metals due to enhanced accessibility of catalytic sites. However, the introduction of mesopores into the AlPO-n materials is not an easy task since their structures are similar to zeolites, and thus they are intrinsically microporous.

Given these facts, it is attractive to synthesize catalyst supports with properties fulfilling these demanding requirements. We explored unconventional syntheses of mesoporous aluminum phosphates and phosphonates by the NHSG routes. These routes, in general, avoid aqueous or protic solvents, and oxygen bridges between metal and phosphorus atoms are formed by condensation of alkoxide, siloxide, chloride, amide, or ester groups. The reactions involve elimination of silylethers [9], alkylsilanes [10], silylamines or alkyl/silylhalides [11–13], or silylesters [14]. A benzyl alcohol route employing metal salts and H_3PO_4 has also been successfully used for metal phosphates [15–17].

Here we report the synthesis of aluminophosphates and aluminophosphonates by non-hydrolytic sol-gel reactions of $Al(NMe_2)_3$ with trimethylsilylated phosphate, phosphonate, and bis-phosphonate esters proceeding by the silylamine elimination of Me_2NSiMe_3. While the principle of this condensation reaction has been reported previously [11], here we widely broaden the choice of precursors, modify reaction conditions, and study the effect of template addition with the aim to prepare and properly characterize materials with tunable porosity. The produced xerogels were studied by solid-state NMR spectroscopy, thermal analysis, infrared spectroscopy, X-ray powder diffraction, and nitrogen physisorption. We show that final porosity depends on organic building blocks as well as the Al:P ratio or applied templates.

Scheme 1: Phosphorus precursors

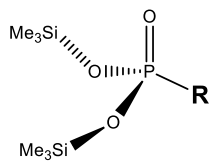

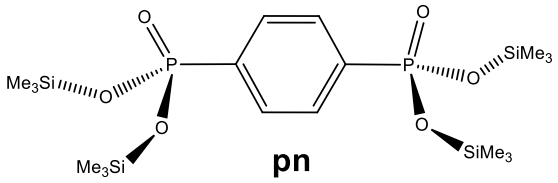

pn

R = OSiMe$_3$ (TTP), Me, ^{t}Bu, Ph

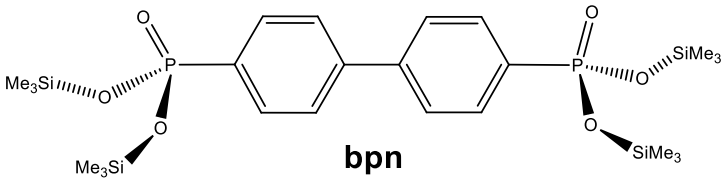

bpn

2. Experimental

2.1. General

All manipulations were performed under dry N_2 using Schlenk techniques or in an M. Braun dry box with both H_2O and O_2 levels below 1 ppm. $Al(NMe_2)_3$ was used as received from the supplier (Merck). Toluene was freshly distilled from Na/benzophenone under N_2, and THF was dried by standard methods and distilled before use. *Tris*(trimethylsilyl)phosphate (TTP) was prepared from H_3PO_4 and Me_3SiCl and vacuum-distilled using standard procedure. $CDCl_3$ was dried by P_2O_5 and vacuum-transferred to an ampoule. $RP(O)(OSiMe_3)_2$ (R = Me, ^{t}Bu, Ph) were prepared by reactions of particular phosphonic acids with Me_3SiCl and then vacuum-distilled. $(Me_3SiO)_2(O)P–X–P(O)(OSiMe_3)_2$ (X = C_6H_4, $(C_6H_4)_2$), were prepared by Arbuzov reactions between $P(OEt)_3$ and Br–X–Br, then Me_3SiBr was added, and the final products were purified by vacuum sublimation. $^{31}P\{^1H\}$ and $^{13}C\{^1H\}$ NMR spectra of phosphonate and bis-phosphonate trimethylsilylesters are shown in Fig. S1–S10.

2.2. Phosphate gels

In a typical synthesis, $Al(NMe_2)_3$ (for exact amounts see Table S1) was dissolved in 40 cm^3 of toluene, and a corresponding amount of tris(trimethylsilyl)phosphate, $OP(OSiMe_3)_3$ (TTP, Scheme 1), was added via syringe leading to compositions with nominal Al:P ratios of 0.8; 0.9; 1.0; 1.1; and 1.4 (Table S1). The gel appeared during the first 15 minutes. The reaction mixture was thoroughly stirred and heated to 80 °C for 168 h. The reaction was stopped after one week, and the gel was dried under a dynamic vacuum for 48 h. A similar process was performed in the case of templated materials where 2.5 g of a 20 % solution of a template (Pluronic P123, F127, Brij 58) in toluene was added into TTP (for exact amounts see Table S1) before adding the corresponding volume of the $Al(NMe_2)_3$ solution in toluene. Dried xerogels were calcined in a horizontal tube furnace under an ambient atmosphere at 500 °C for 4 h with a heating ramp of 5 °C min^{-1}.

The samples of non-templated aluminophosphates were labeled according to their nominal Al:P ratios (e.g., AlP0.8). The templated samples were labeled by the template abbreviation: Pluronic P123 (AlP_P), F127 (AlP_F), Brij 58 (AlP_B). The nominal Al:P ratio in templated samples was 1.0 in all cases. Calcination temperature 500 °C was added to the labels of calcined samples (for example, AlP_P500).

The calcination temperature was optimized according to thermogravimetric measurements, and 500 °C was found sufficient for the complete decomposition of all three templates.

A blank reaction was performed to understand the thermal behavior and stability at elevated temperatures of TTP. The composition of this mixture was $OP(OSiMe_3)_3$ (3.17 mmol) in 20 cm^3 of toluene without the aluminum precursor. The reaction solution was heated to 80 °C, and this temperature was maintained for 168 h. ^{31}P NMR spectra of the reaction mixture were measured after one week, as well as GC MS of byproducts.

2.3. Phosphonate gels

$RP(O)(OSiMe_3)_2$ (R = Me, ^tBu, Ph, for exact amounts see Table S1) was dissolved in 20 cm^3 of toluene and added via syringe to $Al(NMe_2)_3$ (the nominal Al:P stoichiometric ratio was maintained at 2:3 to ensure the equivalent ratio of reacting $NMe_2/OSiMe_3$ groups) dissolved in 20 cm^3 of toluene (Table S1). The gel appeared after 1 h. The reaction mixture was thoroughly stirred and heated to 80 °C for 168 h. Then the reaction was stopped; the gel was dried under a dynamic vacuum until pressure was below $7.5 \cdot 10^{-4}$ Torr, and a yellowish xerogel was obtained. Phosphonate samples were labeled as AlP_*R*, R is an abbreviation of the terminal organic moiety on phosphorus (for example, AlP_Me).

2.4. Bridging bisphosphonate gels

Bridging bisphosphonate gels were prepared in a way similar to the phosphonate gels. The precursor ratio was set to 4:3 (i.e., the Al:P ratio is 2:3), which corresponds to the 1:1 stoichiometric value for the reactive groups $NMe_2/OSiMe_3$ (Table S1). Two phosphorus precursors were applied, namely $(Me_3SiO)_2(O)P–X–P(O)(OSiMe_3)_2$, where X = C_6H_4 and $(C_6H_4)_2$, which were dissolved in 20 cm^3 of toluene and added via syringe to $Al(NMe_2)_3$ dissolved in 20 cm^3 of toluene (Table S1). The gel appeared after 1 h. The reaction mixture was thoroughly stirred and heated to 80 °C for 168 h. Then the reaction was stopped; the gel was dried under a dynamic vacuum until pressure was below $7.5 \cdot 10^{-4}$ Torr, and a yellowish xerogel was obtained. Bisphosphonate samples were labeled as AlP_pn for phenylene, AlP_bpn for biphenylene.

2.5. Characterization

GC MS spectra were obtained on a Thermo Scientific Trace GC Ultra – TSQ Quantum XLS mass spectrometer. TS-SQC column (15 m, 0.25 mm, 0.25 μm) was heated with the following program: 50 °C (0 min), 5 °C min^{-1} up to 80 °C, 15 °C min^{-1} up to 120 °C, 35 °C min^{-1} up to 200 °C (0.5 min). Split mode, injector temperature 200 °C, interface temperature 200 °C, detector temperature 200 °C. The column pressure was set to 31.5 kPa and ionization energy to 70 eV.

Powder XRD diffractograms were recorded on an X'PertPRO diffractometer equipped with a $Co_{K\alpha}$ X-ray tube with a Pt holder or on a GNR Europe 600 diffractometer with a $Co_{K\alpha}$ (1.7903 Å) radiation source. The xerogels were measured on a diffraction-free silicon holder in reflection mode.

For liquid phase $^{13}C\{^1H\}$, and $^{31}P\{^1H\}$ NMR experiments, a Bruker Avance II DRX 300 MHz spectrometer was used. The $^{13}C\{^1H\}$ NMR spectra were referenced to the residual carbon resonances of $CDCl_3$ (77.0 ppm, respectively). The $^{31}P\{^1H\}$ NMR spectra were referenced to [H_3PO_4 (85%)]: δ 0.0 ppm.

The solid-state ^{29}Si and ^{13}C CP MAS and ^{27}Al and ^{31}P MAS NMR spectra were measured on a Bruker Avance III 700 MHz spectrometer with a MAS DVT 700S4 BL4 N-P/H probe. Magic angle spinning rate was set to 5 kHz for ^{29}Si and ^{13}C and 10 kHz for ^{27}Al and ^{31}P spectra. Chemical shifts were referenced externally to ^{31}P δ [H_3PO_4 (85%)]: 0.0 ppm; ^{29}Si δ [$(Me_3SiO)_8Si_8O_{20}$]: 11.72 ppm; ^{13}C δ [adamantane]: 38.68 ppm; ^{27}Al δ [$[Al(H_2O)_6]^{3+}$ (aq. solution)]: 0.0 ppm.

Nitrogen adsorption/desorption experiments were performed at 77 K on a Quantachrome Autosorb-1MP porosimeter. Surface areas (SA) and total pore volumes V_{tot} at p/p_0 = 0.976 were determined by the volumetric technique. Prior to the measurements, the samples were degassed for at least 24 h until the outgassing rate was less than 0.4 Pa min^{-1}. The specific surface area was determined by the multipoint BET method with at least five data points with relative pressures between 0.05 and 0.30. Pore size distributions were calculated with the use of the NLDFT method.

A transmission electron microscope FEI Tecnai G2 was operated at 200 kV acceleration voltage and equipped with a 4k CCD camera FEI Eagle. Data collection is automated by software packages EPU and Tomo.

The degree of condensation was calculated, as shown in Equation 1 [18],

$$DC(\%) = \frac{n_{reacted}}{n_{total}} \qquad \text{Equation 1}$$

in which $n_{reacted}$ is the molar amount of reactive organic groups (NMe_2 and $OSiMe_3$) that condensed according to Equation 2 and were eliminated as silylamine under vacuum. $n_{reacted}$ is obtained by the difference between the weight of starting precursors and the weight of the xerogel, assuming a loss of Me_3SiNMe_2 only. n_{total} represents the molar amount of all reactive organic groups before reaction. Alternatively, DC can also be estimated from the thermogravimetric analysis of the xerogels in the air up to 750 °C, assuming the complete condensation to $AlPO_4$ for the reaction with a 1:1 stoichiometric ratio of Al:P. In other reactions with an excess of Al or P precursors, the formation of corresponding stoichiometric amounts of Al_2O_3, and P_4O_{10}, respectively, have been considered in calculations without the actual presence of these species in the xerogels.

Catalytic experiments were performed as follows. The calcined xerogel catalysts or benchmark catalysts (0.192 g, sieved in the 0.20–0.40 mm particle size range) were diluted with glass beads (0.5-1 mm) in order to keep the volume of the catalyst bed constant (1 mL). The void space of the reactor was filled with silica beads. Catalytic testing was carried out by injecting 0.212 g h^{-1} of absolute ethanol by means of NE-300 syringe pump in a 40 cm^3 min^{-1} flow of N_2 (4.4 mol% of ethanol in N_2). The tests were carried out at atmospheric pressure and weight hourly space velocity WHSV = 1.1 h^{-1}. Temperature was varied stepwise in the range from 210 to 340 °C by steps of 35 °C. One step consisted of (i) heating ramp (5 °C min^{-1}) and stabilization at the set temperature (21 min) and (ii) steady temperature state (56 min). The analysis of the effluent gas was carried out by a VARIAN 3800 Gas Chromatograph (5 injections at each temperature) equipped with a flame ionization detector (FID) and a Rt-U-BOND column (Restek, 30 m long, internal diameter 0.25 mm, film thickness 8 µm).

3. Results and discussion

3.1. Condensation reactions

The reactions provided yellowish gels in 40 min after reagent mixing. The mixtures were heated to 80 °C for 168 h. In all cases, Me_3SiNMe_2 was the major volatile byproduct identified by GC MS (RT 0.70 min, m/z: 117, 102, 59). Elimination of silylamine is consistent with the expected non-hydrolytic sol-gel condensation in Equation 2.

$$Al–NMe_2 + Me_3Si\text{-}O–P \rightarrow Me_2N–SiMe_3 + Al–O–P \quad \text{Equation 2}$$

Hexamethyldisiloxane was identified as a minor byproduct (RT 0.74 min, m/z: 149, 148, 147). The silylamine:hexamethyldisiloxane ratios were above 3.4, with no evident dependency on chosen precursors, templates, or stoichiometric ratios. Hexamethyldisiloxane presumably results from condensation between the $P–OSiMe_3$ groups leading to P–O–P bridges (Equation 3). That notion was substantiated by a blank reaction in which $OP(OSiMe_3)_3$ in toluene was heated to 80 °C, and this temperature was kept for 168 h. Hexamethyldisiloxane was identified by GC MS, and the ^{31}P NMR spectra showed two resonances at –14.0 ppm and –25.4 ppm, which were assigned to diphosphate and tris(trimethylsilyl) phosphate, respectively. Only 3.8 % of all phosphate was transformed into diphosphate.

$$P–OSiMe_3 + Me_3Si\text{-}O–P \rightarrow Me_3SiOSiMe_3 + P–O–P \quad \text{Equation 3}$$

The residual masses found by TGA of the samples in air agree with the residual masses calculated from the degrees of condensation in Table 1, assuming that the residue is composed of $AlPO_4$ and the excess of either Al or P is stoichiometrically accounted for as Al_2O_3 or P_4O_{10}, depending on the Al:P ratio (see Table S1). Two separate mass losses were identified in cases where phosphonates were used as the phosphorous precursors (Fig. 1). The first mass loss (below 400 °C) is ascribed to the loss of the $SiMe_3$ residual groups, the second mass loss (above 400 °C) to the loss of the NMe_2 and aromatic bridging or methyl groups.

The degrees of condensation reported in Table 1 are quite high (82–91 %) for the samples prepared with stoichiometric amount of reactants according to Equation 2, indicating the formation of highly condensed Al–O–P networks. Conversely, they are lower (73–79 %) for the aluminum phosphate samples prepared with an excess of aluminum or phosphate precursors (AlPx samples with $x \neq 1$).

Table 1 Residual masses (RM) after TG analysis and the calculated values of RM from the degree of condensation DC (%)

Sample	RM_{TG} (%)	RM_{calc} (%)	DC (%)
AlP0.8	74.5	59.8	74
AlP0.9	75.2	64.9	79
AlP1.0	78.9	67.4	91
AlP1.1	77.5	63.6	80
AlP1.4	78.6	65.8	73
AlP_P	42.1	40.4	83
AlP_B	46.6	42.6	83
AlP_F	42.0	40.1	82
AlP_Me	87.9	81.7	86

AlP_Bu	70.5	56.9	87
AlP_Ph	70.0	52.6	89
AlP_pn	67.5	65.6	77
AlP_bpn	60.8	55.6	75

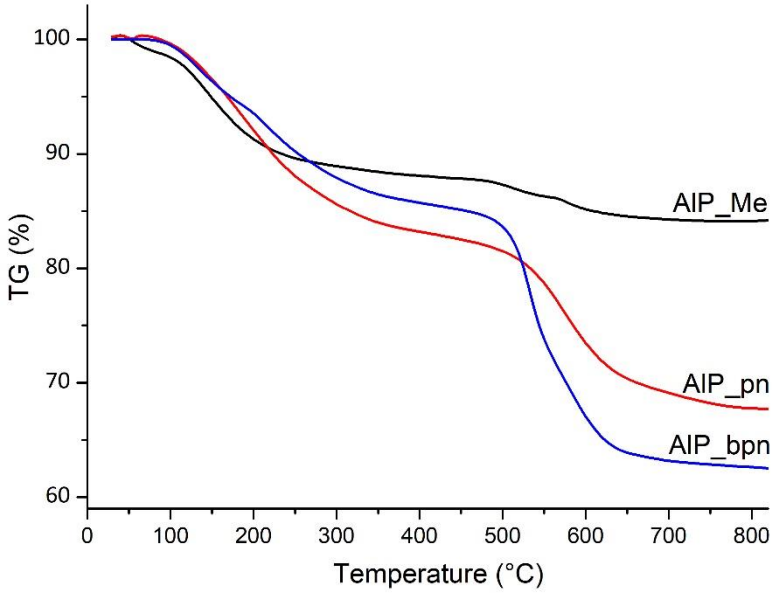

Fig. 1. Thermogravimetric traces to 800 °C of samples AlP_Me (top), AlP_pn (middle), and AlP_bpn (bottom)

3.2. Structure of the xerogels

All samples, including the aluminophosphates calcined at 500 °C, were amorphous to XRD (Fig. S11). This could be related to the irreversibility of the condensation reaction (Equation 2) carried out under non-hydrolytic conditions at relatively low temperature (80 °C), which hinders the rearrangement of the formed Al–O–P bonds. The network is prevented from reaching thermodynamically stable state and thus its crystallization is inhibited. Formation of crystalline zeolitic aluminophosphates requires prolonged hydrothermal treatment. The samples stayed amorphous up to 700 °C and crystallized at 900 °C to a hexagonal tridymite phase (COD 96-201-2012, Fig. S12) in agreement with other literature reports [19].

NMR spectroscopy

The ^{29}Si CP MAS NMR spectra (Fig. 2) show a major resonance at 20 ppm arising from the residual Me_3SiO groups bonded to the P atoms and a smaller peak around 1.0 ppm which could be assigned to the same group bonded to the Al atoms. This result could mean that a limited ligand exchange (Equation 4) takes place in the reaction system. A similar ligand exchange was observed between $OP(OPh)_3$ and $Al(NMe_2)_3$ [11]. Such a ligand exchange, followed by a further condensation reaction, would release $Me_3SiOSiMe_3$ identified among byproducts (Equation 5).

$$P{-}OSiMe_3 + Me_2N{-}Al \rightarrow P{-}NMe_2 + Me_3SiO{-}Al$$ Equation 4

$$Al{-}OSiMe_3 + Me_3SiO{-}P \rightarrow Al{-}O{-}P + Me_3SiOSiMe_3$$ Equation 5

The ^{13}C CP MAS NMR spectra of all samples (Fig. 3) contained a resonance at 3 ppm, assigned to the $Si(CH_3)_3$ groups, and a second resonance at 42 ppm for $N(CH_3)_2$. Additional signals in the ^{13}C CP MAS NMR spectra of individual aluminophosphonates are as follows: a CH_3–P signal for AlP_Me is shifted to 15 ppm, AlP_Ph displays signals in the phenyl carbon range at 125–140 ppm, and AlP_Bu shows two signals at 28 ppm and 33 ppm assigned to methyl and quaternary carbons, respectively, in the ^{t}Bu group. The spectra of the bisphosphonate xerogels display extra signals at the 120–130 ppm aromatic region.

According to the ^{27}Al MAS NMR spectra, the coordination environment of aluminum varies with the aluminophosphate xerogel composition (Fig. 4). The 1:1 stoichiometric ratio of Al and P or an excess of phosphorus leads mainly to four-coordinated aluminum. The samples prepared with excess $Al(NMe_2)_3$ exhibit two types of four-coordinated aluminum centers. The first resonance at 42 ppm is ascribed to AlO_4 detected in all samples, the second one at 60 ppm possibly corresponds to the AlO_3N sites, related to the residual dimethylamide groups. Tris(dimethylamido)aluminum with a dimeric structure featuring two four-coordinated Al centers has a ^{27}Al chemical shift of 110 ppm [20]. Templated phosphates show three well-defined resonances at 42, 8, –12 ppm, which belong to four-, five-, and six-coordinated aluminum (Fig. S13). The ^{27}Al MAS NMR spectra of phosphonates and bisphosphonates samples show four resonances at 43, 9, –13, and –19 ppm assigned to AlO_4, AlO_5, and two types of AlO_6, respectively (Fig. S14). The signals for the AlO_4 species are the most intense. It is known that four- and five- coordinated aluminum centers are Lewis acidic sites. Its acidic properties were tested by the ethanol dehydration reaction (vide infra).

The resonances of the PO_4 groups in the ^{31}P MAS NMR spectra are at around –26 ppm for all phosphate xerogels (Fig. S15), suggesting that the environment of PO_4 centers changes only negligibly for various Al:P ratios. Phosphorus shifts in the range between –20 and –30 ppm are typical for $P(OAl)_4$ moieties in aluminophosphates in general [21,22]. The ^{31}P chemical shifts of the aluminum phosphonate samples are found at 0 ppm. For bridging bisphosphonates, the two bridging parts are similar aromatics so that ^{31}P chemical shifts are the same for both samples and appear at –3 ppm.

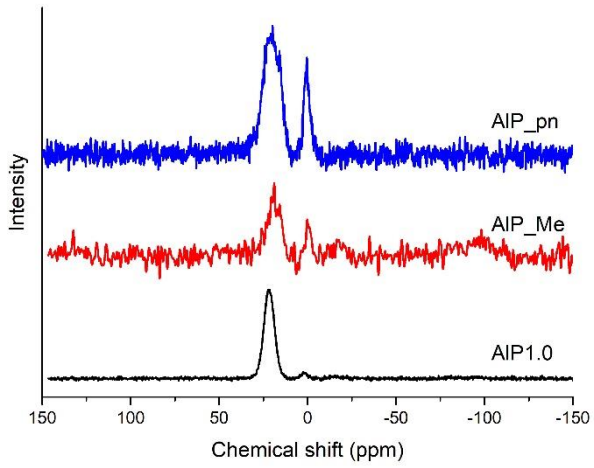

Fig. 2. ^{29}Si CP MAS NMR spectra of AlP1.0 (bottom), AlP_Me (middle), and AlP_pn (top)

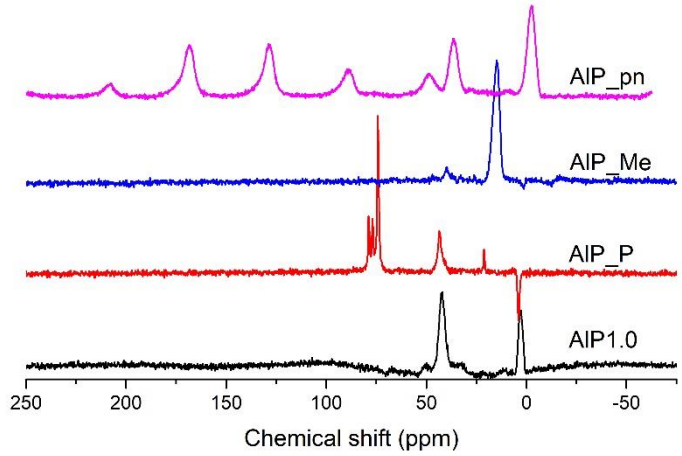

Fig. 3. ^{13}C CP MAS NMR spectra of AlP_pn and ^{13}C CP TOSS NMR spectra of AlP_Me, AlP_P, and AlP1.0

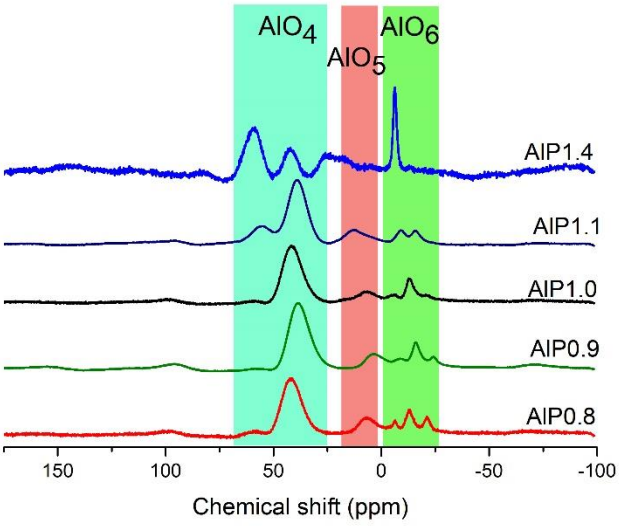

Fig. 4. ^{27}Al MAS NMR spectra of AlP1.4, AlP1.1, AlP1.0, AlP0.9, AlP0.8 (from top to bottom), rotation speed 10 kHz

Infrared spectroscopy

Infrared spectroscopy was used as a complementary method for structure characterization. The spectra were similar in the group of phosphate xerogels. For example, samples AlP0.8, AlP1.0, and AlP1.4 in

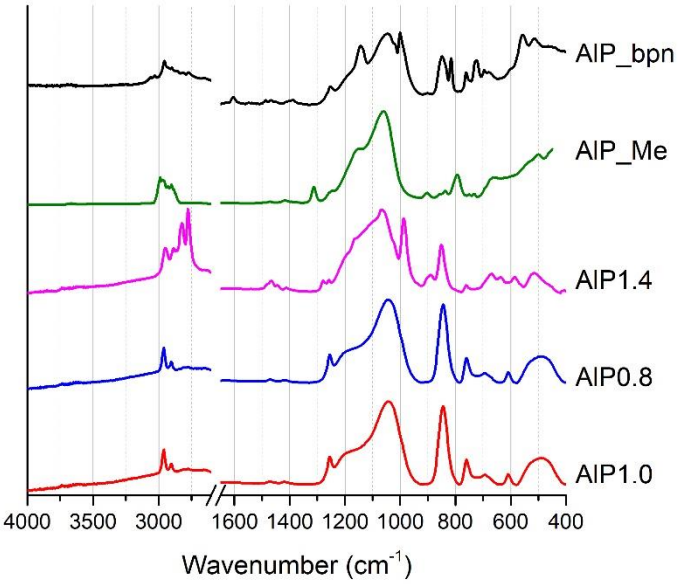

Fig. 5 have an intense peak at ≈1044 cm^{-1}, which demonstrates the presence of expected Al–O–P bonds. We can observe absorption bands specific for the $Si(CH_3)_3$ groups (760, 846, and 1255 cm^{-1}). There is also a vibration band at 2968 cm^{-1}, which is characteristic of C-H stretching in the CH_3 groups. The presence of trimethylsilyl residual groups is thus proven by these vibration bands. The sample prepared with an excess of the aluminum precursor (AlP1.4) had an intense vibration at 987 cm^{-1}, and a shoulder at 1156 cm^{-1}, assigned to Al–N and N–C stretches, respectively. These data point to the presence of residual amide groups. In the case of the phosphate samples, vibration bands related to residual groups and templates disappeared after calcination.

The methyl phosphonate sample is distinguished by one more shoulder at the Al–O–P band. It was located at 1312 cm^{-1} and assigned to the vibration of P–C bonds. Aromatic phosphonates (AlP_bpn:

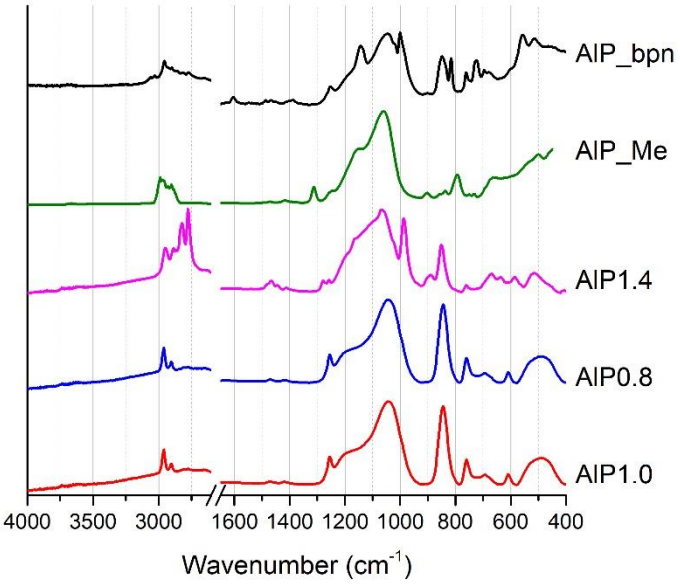

Fig. 5) have a very weak vibration of conjugated C=C bonds around 1605 cm^{-1} and a weak vibration at 3029 cm^{-1} typical for aromatic C–H bond, which confirms the presence aromatic bridges. Thus, the IR spectra support the data from the MAS NMR spectroscopy.

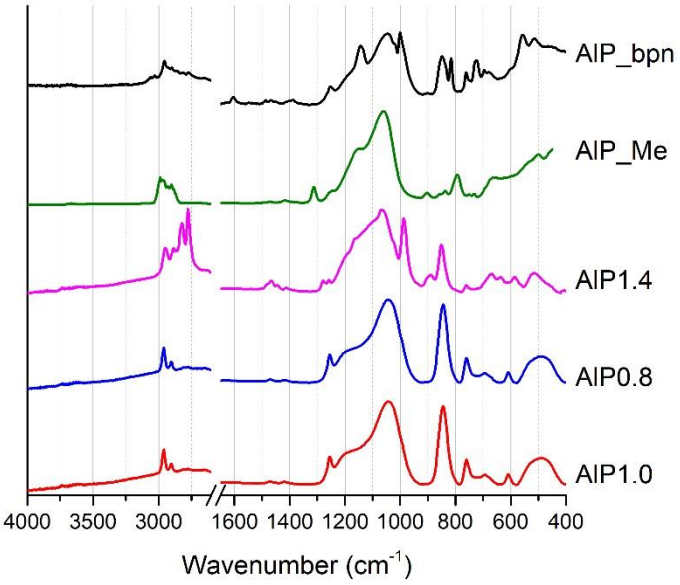

Fig. 5. IR spectra of selected samples AlP_bpn, AlP_Me, AlP1.4, AlP0.8, AlP1.0 (from top to bottom). The 2600–1650 cm^{-1} region is omitted since there were no vibration bands. The 4000–2600 cm^{-1} region is magnified 5x

3.3. Texture of the samples

Non-templated and templated aluminophosphates

In the case of aluminophosphate samples with different Al:P ratios (AlP0.8 to AlP1.4), nitrogen physisorption measurements on dried xerogels (before calcination) revealed adsorption/desorption isotherms belonging to type IV, which is typical of mesoporous materials (Fig. 6a). Their hystereses are spread out over the whole p/p_0 range. The TEM image of the sample AlP1.0 reveals a wormhole texture (Fig. S16).

We found that an excess of the aluminum precursor led to higher specific surface areas (Table 2): for the Al:P ratios of 1.1 and 1.4, the SA is 800 $m^2 g^{-1}$, and it decreases to ≈650 $m^2 g^{-1}$ for the Al:P ratios of 1.0 or lower.

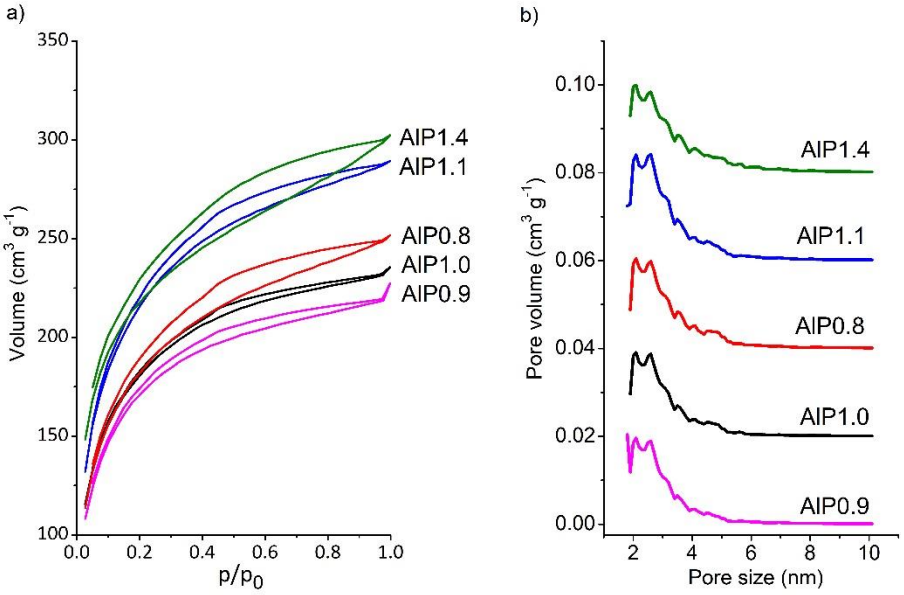

Fig. 6. a) Nitrogen adsorption/desorption isotherms of aluminophosphate samples and b) corresponding graphs of pore size distributions, offset for each line was set to 0.02 $cm^3 g^{-1}$

NLDFT pore size distributions were similar for all aluminophosphate xerogels with various Al:P ratios (Fig. 6b) and they show mesopores in the range from 2.0 to 6.0 nm (Table 2).

After calcination at 500 °C, even though all samples remained amorphous, their specific surface area and pore volumes were drastically reduced (Table 2), indicating a practically complete collapse of the pore network.

In order to increase the mesoporosity of calcined aluminophosphate AlP1.0 samples, three different templates were used in their synthesis, Pluronic P123, F127, and Brij 58. These templates differ in the ratio of polar and nonpolar parts and in the molecular weight. Pluronic F127 is the most polar template. The weight of the templates used in the reaction resulted from our earlier experience and was set to one-tenth of the theoretical weight of the aluminum phosphate product (i.e., when 100 % degree of condensation is reached). The porosity of samples AlP_P, _F, and _B was measured after removal of the templates by calcination. Obtained isotherms and calculated pore size distributions are shown in Fig. 7.

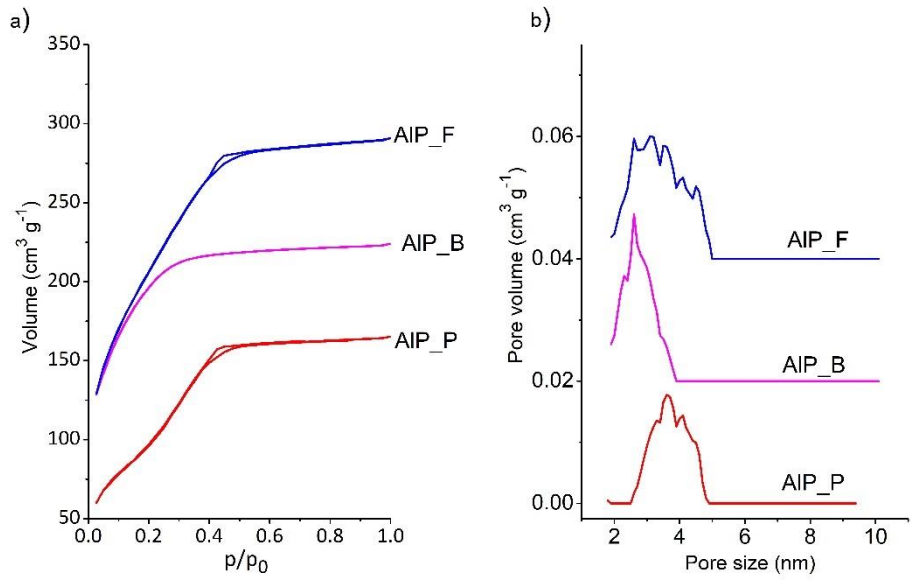

Fig. 7. a) Nitrogen adsorption/desorption isotherms of templated aluminophosphate samples AlP_F, AlP_B, and AlP_P (from top to bottom) and b) corresponding graphs of pore size distributions, with offset equal to 0.02 $cm^3\ g^{-1}$ for each line

As shown in Table 2, the use of a template significantly improved the texture of the calcined aluminophosphate xerogels in comparison to collapsed non-templated samples. Depending on the template, specific surface areas ranged from 340 to 750 $m^2\ g^{-1}$ and total pore volume from 0.25 to 0.45 $cm^3\ g^{-1}$. Templates apparently stabilize the network of pores during calcination and maintain the high surface area and pore volume in calcined samples.

When Brij 58 was used as a templating agent, an isotherm of type I with no evident hysteresis was obtained, which may suggest the presence of microporosity in the material. However, the pore size distribution is in the mesopore range. Better results were obtained with Pluronic P123, which led to uniform mesopores with diameters around 3.7 nm and a SA of 340 $m^2\ g^{-1}$. The isotherm has signs of type IV with H2 hysteresis. The best template seems to be Pluronic F127, which led to a high SA of 750 $m^2\ g^{-1}$, and its pore sizes are distributed predominantly into mesopores with a mode of pore sizes of 3.2 nm. The isotherm of this sample belongs to type IV with H2 hysteresis.

Table 2 Composition (Al:P ratio), degree of condensation (DC), and characteristic textural data of aluminophosphate and aluminophosphonate xerogels

Sample	Al:P	Template	Org. moiety at P	DC (%)	Average pore size (nm)	NLDFT mode pore size (nm)	Pore volume ($cm^3 g^{-1}$)	Surface area ($m^2 g^{-1}$)
AlP0.8	0.8	—	—	74	2.3	2.0	0.39	670
AlP0.9	0.9	—	—	79	2.1	2.0	0.34	630
AlP1.0	1.0	—	—	91	2.2	2.0	0.36	670
AlP1.1	1.1	—	—	80	2.2	2.6	0.45	800
AlP1.4	1.4	—	—	73	2.3	2.0	0.46	800
AlP0.8-500	0.8	—	—	74	–	–	0	1
AlP0.9-500	0.9	—	—	79	–	–	0	1
AlP1.0-500	1.0	—	—	91	–	–	0	0
AlP1.1-500	1.1	—	—	80	–	–	0	0
AlP1.4-500	1.4	—	—	73	–	–	0	2
AlP_P500	1.0	P123	—	83	2.6	3.7	0.25	340
AlP_B500	1.0	Brij 58	—	83	1.9	2.6	0.35	720
AlP_F500	1.0	F127	—	82	2.4	3.2	0.45	750
AlP_Me	0.66	—	Me-	86	4.3	3.2	1.04	970
AlP_Bu	0.66	—	^{t}Bu-	87	2.2	1.3	0.33	590
AlP_Ph	0.66	—	Ph-	89	2.3	2.6	0.32	550
AlP_pn	0.66	—	-C_6H_4-	77	3.7	5.3	0.93	1030
AlP_bpn	0.66	—	-$(C_6H_4)_2$-	75	2.6	5.9	0.54	840

Aluminophosphonate xerogels

The texture of the aluminum phosphonate xerogels depends on the nature of the organic group of the phosphonate units. The porous character of the aluminum tert-butyl phosphonate (AlP_Bu) and phenylphosphonate (AlP_Ph) xerogels was very similar as they feature a specific surface area of 590 and 550 $m^2 g^{-1}$, respectively. Their type I isotherms are almost overlapped, and they gradually increase at higher pressures (Fig. 8a). The aluminum methylphosphonate sample (AlP_Me) exhibited a much larger specific surface area (970 $m^2 g^{-1}$) and three times higher total pore volume (1.04 $cm^3 g^{-1}$) than AlP_Bu and AlP_Ph. Its isotherm shape is similar to isotherm type I, with hysteresis over the whole p/p_0 range. Pore size distributions of all phosphonate xerogels have bimodal characteristics with maxima at 3 nm and 5 nm (Fig. 8b). As can be seen in Fig. 9, the porous wormhole structure is also seen in the TEM image without any crystallinity or ordering.

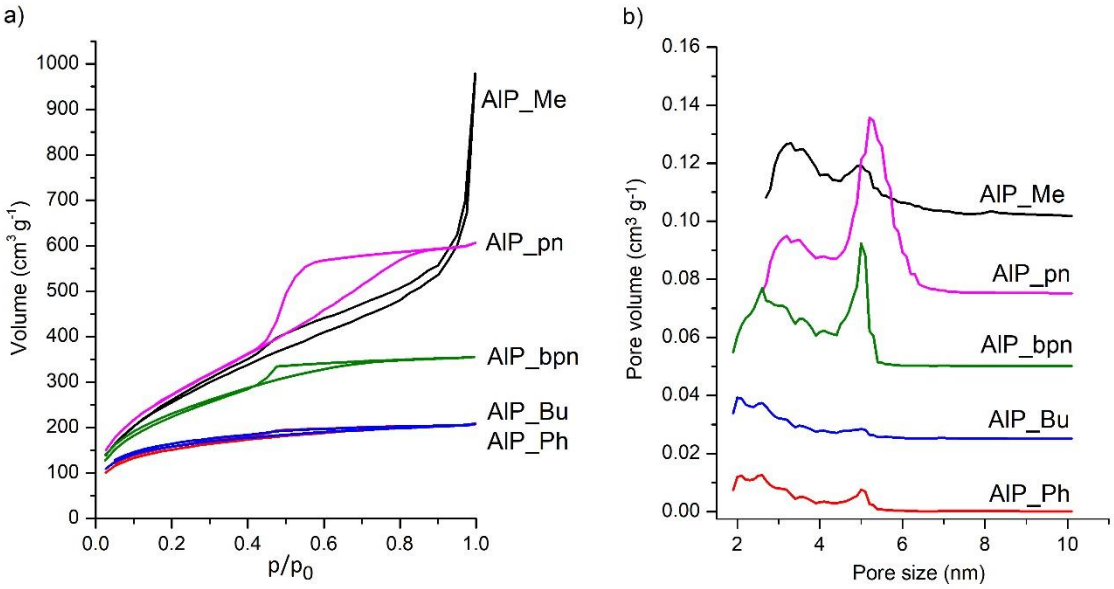

Fig. 8. a) Adsorption/desorption isotherms of aluminophosphonate samples and b) corresponding graphs of pore size distributions with offset equal to 0.025 $cm^3 g^{-1}$ for each line

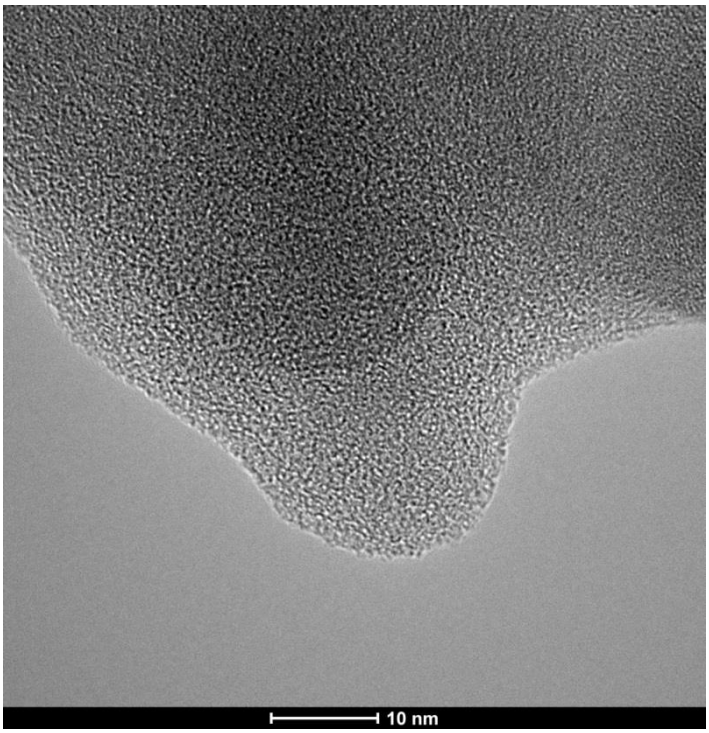

Fig. 9. The TEM image of AlP_Me sample

Bridging aluminum bisphosphonate xerogels

Both xerogels prepared with bridged bisphosphonates (AlP_pn and AlP_bpn) showed clear type IV physisorption isotherms with an H2 hysteresis typical for disordered mesopores with ink bottle shape (Fig. 8a). Both samples have large surface areas. The pore size is not proportional to the length of the spacer; thus, the NLDFT mode of pore sizes of the sample prepared with the biphenylene spacer is comparable to that of the sample with the shorter phenylene spacer (Table 2). The AlP_pn sample was examined by TEM (Fig. S17). As can be seen in the image, there are many pores randomly assembled with a uniform diameter of a few nanometers pointing to a worm-hole type porosity.

3.4. Ethanol conversion catalysis

The templated aluminophosphate sample AlP_F500 was tested as a catalyst for the gas-phase ethanol dehydration in the temperature range between 210 and 345 °C and compared to the three benchmark catalysts – amorphous silica-alumina catalyst support (SACS), γ-alumina (Al_2O_3) and crystalline zeolite HZSM-5 – in order to describe the acidic properties of the prepared materials [23,24]. There are several reasons for choosing AlP_F500 as the representative sample. It has medium high surface area and pore volume. The pores should be accessible thanks to high percentage of mesoporosity. And it is calcined at higher temperature than that required for catalysis which ensures the stability during tests.

The major products of the catalytic reaction were ethylene and diethylether with carbon balances reaching 88–100 %. No other products were observed except for HZSM-5 and Al_2O_3, which produced low amounts of acetaldehyde, propene, and butenes (≈0.5–2 % in selectivity to these by-products in total). Sample AlP_F500 produced only negligible amount of acetaldehyde (0.3 % in selectivity at 290–325 °C).

In a screening on the effect of temperature, we observed that aluminophosphate was significantly more active than the commercial SACS and Al_2O_3 samples at low temperature (210 °C). At higher temperatures (280 °C and above), the ethanol conversion over these three catalysts was similar. Expectedly, SACS, AlP_F500 and alumina were outperformed by highly active HZSM-5 in the whole temperature range, Fig. 10.

In fact, HZSM-5 is known as the state-of-the-art catalyst for ethanol dehydration to ethylene. At low temperature it yields mostly diethylether and already significant amounts of ethylene, due to its strong acidity [25]. At 240 °C, a complete conversion of ethanol to ethylene is observed, Fig. 11a. Yet, this catalyst is also prone to coking, especially at high temperature, so it is interesting to screen for formulations that exhibit a lower acidity. In this scenario, Al_2O_3 and SACS are the useful benchmark. These catalysts are quite selective for diethylether at moderate temperature (210 °C) and become highly selective for ethylene only above 300 °C.

In terms of ethylene production, AlP_F500 behaves similarly to these benchmarks, reaching high yields at high temperature only indicating the presence of weak acid sites. Interestingly, however, this catalyst is both highly active and fully selective to diethyl ether at low temperature (210 °C) (see also Fig. S18). Thus, a diethylether yield of 63 % is reached, similar to the one obtained with HZSM-5, but without the concomitant production of ethylene, Fig. 11b. AlP_F500 is therefore identified as a good candidate for the selective upgrading of ethanol to diethylether at low temperature.

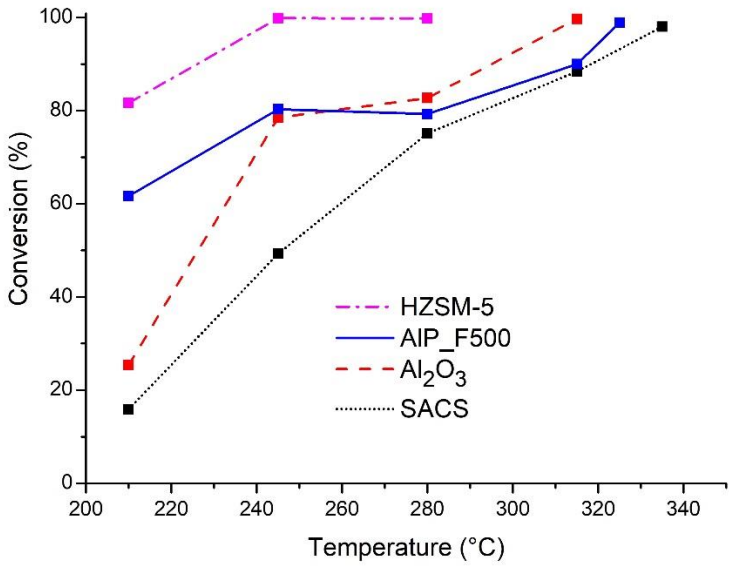

Fig. 10. The comparison of conversion of AlP_F500 and three commercial benchmarks

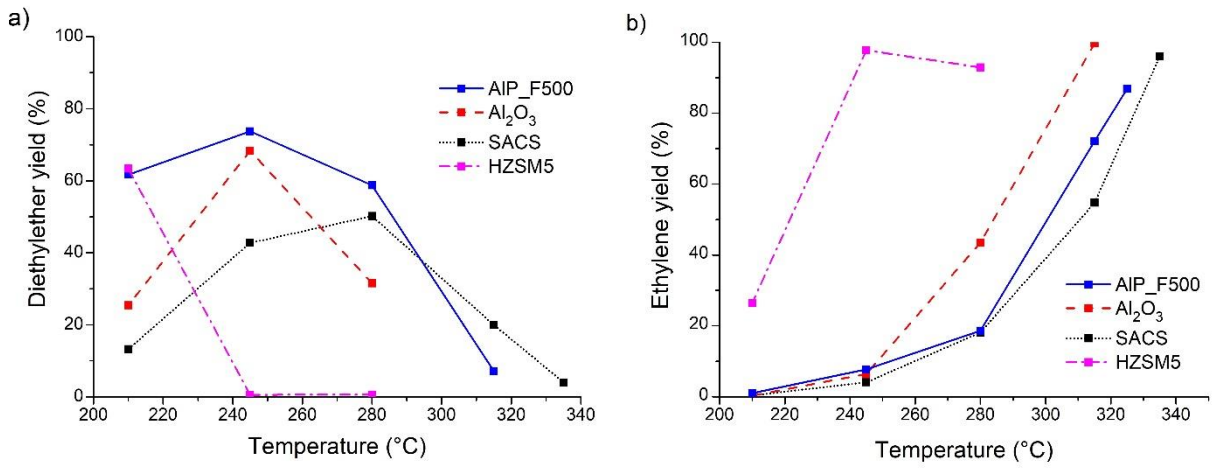

Fig. 11. The comparison of diethylether (a) and ethylene (b) yields for AlP_F500 and three commercial benchmarks

4. Conclusions

Aluminophosphates and aluminophosphonates were synthesized under non-hydrolytic sol-gel conditions by silylamine elimination from tris(dimethylamido)aluminum and different phosphorus precursors (silylated phosphates, alkylphosphonates, and bridged bisphosphonates). Well-condensed networks with considerable porosity resulted from the polycondensation reactions between dimethylamido and trimethysiloxy groups. Porous materials can be synthesized without templates. Materials prepared this way are homogenous at the atomic scale; they are also amorphous because the condensation reaction is irreversible, and newly formed Al–O–P bonds have only negligible dissociation constant (at synthesis conditions), so the gel network has no possibility for self-rearranging.

If a mesoporous material is a goal, the F127 template gives excellent characteristics among the other templates, including SA of 750 $m^2\ g^{-1}$ and pore volume of 0.45 $cm^3\ g^{-1}$. The templates have one more important feature, the thermal stability of xerogels during calcination is increased, and the excellent porous properties are maintained after calcination at 500 °C.

In the system of $Al(NMe_2)_3$ and $RP(O)(OSiMe_3)_2$ (where R = Me, ^tBu, Ph) and $(Me_3SiO)_2P(O)–X–P(O)(OSiMe_3)_2$ (where X = C_6H_4, $(C_6H_4)_2$) we observed only facile condensation producing Al–O–P bonds and elimination of byproducts. The IR spectroscopy verified the presence of the Al–O–P bonds in all samples and the C–P bonds in organic-inorganic hybrid xerogels. The most remarkable results are those of samples with the P–C bond. The SA of 1030 $m^2\ g^{-1}$ can be reached when organo-bridging bisphosphonates are used. The pore volume of 0.93 $cm^3\ g^{-1}$ is entirely in the mesoporous range. If methylphosphonate is used, the surface up to 970 $m^2\ g^{-1}$ is attained, and the pore volume reached up to 1.04 $cm^3\ g^{-1}$. All synthesized aluminophosphonates are characterized by high specific surface areas and the total pore volumes even without any structure-directing agents. It implies that convectional templates can be replaced by wisely chosen organic-inorganic hybrid precursors, and improved parameters can be obtained. We suppose this hypothesis is applicable in other systems besides aluminophosphonates.

Xerogels have integrated [AlO_4] and [AlO_5] species, which is one of the characteristics of effective catalysts. Therefore, these materials have the potential to be industrially useful. Other properties, such as effectiveness, lifetime, the ability of regeneration, and Lewis/Brønsted acid sites, need further studies.

We are not able to separate the template removal process from removing the residual groups by simple thermal calcination in an ambient atmosphere so far. The ability to remove templates, but not residual groups, is crucial for catalyst preparation because divalent or tetravalent metal cations can react with the surface groups, and in this way, they can be easily incorporated into materials. This grafting process is an area for further research.

The catalytic tests (gas phase ethanol dehydration) showed that AlP_F500 behaved similarly to mildly acidic γ-Al_2O_3 and amorphous silica-alumina in terms of ethanol conversion, diethylether and ethylene selectivity. The product of ethanol dehydrogenation (acetaldehyde) was not observed (or in very small amounts) proving unambiguously the absence of redox sites. We can thus easily envisage other catalytic applications requiring mild acidity, high mesoporosity, and thermal durability of NHSG prepared aluminophosphate materials.

Acknowledgments

This research has been financially supported by the MEYS CR under the project Mobility FRANCE 7AMB17FR050 and CEITEC 2020 (LQ1601). CIISB research infrastructure project LM2018127 funded by the MEYS CR is gratefully acknowledged for the financial support of the measurements at the CEITEC MU CF Cryo-electron Microscopy and Tomography. The authors thank the Barrande Mobility project, which supported the stay of PM in Montpellier.

References

[1] A. Styskalik, D. Skoda, C. Barnes, J. Pinkas, The Power of Non-Hydrolytic Sol-Gel Chemistry: A Review, Catalysts. 7 (2017). https://doi.org/10.3390/catal7060168.

[2] A. Vioux, H.P. Mutin, Nonhydrolytic Sol-Gel Technology, in: L. Klein, M. Aparicio, A. Jitianu (Eds.), Handb. Sol-Gel Sci. Technol., 1st ed., Springer, Cham, 2018: pp. 1039–1065.

[3] C. Sanchez, P. Belleville, M. Popall, L. Nicole, Applications of advanced hybrid organic–inorganic nanomaterials: from laboratory to market, Chem. Soc. Rev. 40 (2011) 696–753. https://doi.org/10.1039/c0cs00136h.

[4] J.J. Kirkland, M.A. van Straten, H.A. Claessens, High pH mobile phase effects on silica-based reversed-phase high-performance liquid chromatographic columns, J. Chromatogr. A. 691 (1995) 3–19. https://doi.org/10.1016/0021-9673(94)00631-I.

[5] S.G. Hedge, P. Ratnasamy, L.M. Kustov, V.B. Kazansky, Acidity and catalytic activity of SAPO-5 and AlPO-5 molecular sieves, Zeolites. 8 (1988) 137–141. https://doi.org/10.1016/S0144-2449(88)80080-0.

[6] X. Zhao, Z. Sun, Z. Zhu, A. Li, G. Li, X. Wang, Evaluation of iron-containing aluminophosphate

molecular sieve catalysts prepared by different methods for phenol hydroxylation, Catal. Letters. 143 (2013) 657–665. https://doi.org/10.1007/s10562-013-1027-1.

[7] J. Chen, J.M. Thomas, MAPO-18 (Mg, Zn, Co): a new family of catalysts for the conversion of methanol to light olefins, J. Chem. Soc. Chem. Commun. 18 (1994) 603–604. https://doi.org/10.1039/c39940000603.

[8] T. Mishra, K.M. Parida, S.B. Rao, Transition metal promoted AlPO4 catalyst 2. The catalytic activity of M0.05Al0.95PO4 for alcohol conversion and cumene cracking/dehydrogenation reactions, Appl. Catal. A Gen. 166 (1998) 115–122. https://doi.org/10.1016/S0926-860X(98)80006-9.

[9] G. Guerrero, P.H. Mutin, A. Vioux, Mixed Nonhydrolytic / Hydrolytic Sol − Gel Routes to Novel Metal Oxide / Phosphonate Hybrids, Mater. Res. 47 (2000) 1268–1272. https://doi.org/10.1021/cm991125.

[10] J. Pinkas, D. Chakraborty, Y. Yang, R. Murugavel, M. Noltemeyer, H.W. Roesky, Reactions of Trialkyl Phosphates with Trialkyls of Aluminum and Gallium: New Route to Alumino- and Gallophosphate Compounds via Dealkylsilylation †, Organometallics. 18 (1999) 523–528. https://doi.org/10.1021/om9806702.

[11] J. Pinkas, H. Wessel, Y. Yang, M.L. Montero, M. Noltemeyer, M. Fröba, H.W. Roesky, Reactions of Phosphoric Acid Triesters with Aluminum and Gallium Amides, Inorg. Chem. 37 (1998) 2450–2457. https://doi.org/10.1021/ic9713036.

[12] M.L. Vona, E. Traversa, S. Licoccia, Non-Hydrolytic Routes for the Synthesis of NASICON, J. Sol-Gel Sci. Technol. 19 (2000) 463–467. https://doi.org/10.1023/A:1008707815750.

[13] R.J.P. Corriu, D. Leclercq, P.H. Mutin, L. Sarlin, A. Vioux, Nonhydrolytic sol-gel routes to layered metal(IV) and silicon phosphonates, J. Mater. Chem. 8 (1998) 1827–1833. https://doi.org/10.1039/a803755h.

[14] A. Styskalik, D. Skoda, Z. Moravec, J.G. Abbott, C.E. Barnes, J. Pinkas, Synthesis of homogeneous silicophosphate xerogels by non-hydrolytic condensation reactions, Microporous Mesoporous Mater. 197 (2014) 204–212. https://doi.org/10.1016/j.micromeso.2014.06.019.

[15] M.G. Willinger, G. Clavel, W. Di, N. Pinna, A general soft-chemistry route to metal phosphate nanocrystals, J. Ind. Eng. Chem. 15 (2009) 883–887. https://doi.org/10.1016/j.jiec.2009.09.017.

[16] I. Bilecka, A. Hintennach, I. Djerdj, P. Novák, M. Niederberger, Efficient microwave-assisted synthesis of LiFePO4 mesocrystals with high cycling stability, J. Mater. Chem. 19 (2009) 5125–5128. https://doi.org/10.1039/b909545d.

[17] I. Bilecka, A. Hintennach, M.D. Rossell, D. Xie, P. Novák, M. Niederberger, Microwave-assisted solution synthesis of doped LiFePO4with high specific charge and outstanding cycling performance, J. Mater. Chem. 21 (2011) 5881–5890. https://doi.org/10.1039/c0jm03476b.

[18] A. Styskalik, D. Skoda, Z. Moravec, M. Babiak, C.E. Barnes, J. Pinkas, Control of micro/mesoporosity in non-hydrolytic hybrid silicophosphate xerogels, J. Mater. Chem. A. 3 (2015) 7477–7487. https://doi.org/10.1039/C4TA06823H.

[19] G. Liu, Z. Wang, M. Jia, X. Zou, X. Zhu, W. Zhang, D. Jiang, Thermally Stable Amorphous Mesoporous Aluminophosphates with Controllable P/Al Ratio: Synthesis, Characterization,

and Catalytic Performance for Selective O-Methylation of Catechol, J. Phys. Chem. B. 110 (2006) 16953–16960. https://doi.org/10.1021/jp062824u.

[20] P.L. Bryant, C.R. Harwell, A.A. Mrse, E.F. Emery, Z. Gan, T. Caldwell, A.P. Reyes, P. Kuhns, D.W. Hoyt, L.S. Simeral, R.W. Hall, L.G. Butler, Structural Characterization of MAO and Related Aluminum Complexes. 1. Solid-State 27 Al NMR with Comparison to EFG Tensors from ab Initio Molecular Orbital Calculations, J. Am. Chem. Soc. 123 (2001) 12009–12017. https://doi.org/10.1021/ja011092a.

[21] J.M. Campelo, M. Jaraba, D. Luna, R. Luque, J.M. Marinas, A. Romero, J. Navio, M. Macias, Effect of Phosphate Precursor and Organic Additives on the Structural and Catalytic Properties of Amorphous Mesoporous AlPO 4 Materials, Chem. Mater. 15 (2003) 3352–3364. https://doi.org/10.1021/cm030206+.

[22] M. Tiemann, M. Schulz, C. Jager, M. Froeba, Mesoporous aluminophosphate molecular sieves synthesized under nonaqueous conditions, Chem. Mater. 13 (2001) 2885–2891. https://doi.org/10.1021/cm011044p.

[23] T.K. Phung, G. Busca, Diethyl ether cracking and ethanol dehydration: Acid catalysis and reaction paths, Chem. Eng. J. 272 (2015) 92–101. https://doi.org/10.1016/j.cej.2015.03.008.

[24] F. Bautista, 1-Butanol dehydration on AlPO4 and modified AlPO4: catalytic behaviour and deactivation, Appl. Catal. A Gen. 130 (1995) 47–65. https://doi.org/10.1016/0926-860X(95)00106-9.

[25] A. Styskalik, V. Vykoukal, L. Fusaro, C. Aprile, D.P. Debecker, Mildly acidic aluminosilicate catalysts for stable performance in ethanol dehydration, Appl. Catal. B Environ. 271 (2020) 118926. https://doi.org/10.1016/j.apcatb.2020.118926.

Supporting Information

Synthesis of High Surface Area Aluminophosphate and -phosphonate Xerogels by Non-Hydrolytic Sol-Gel Reactions

Petr Machac,[a] Johan G. Alauzun,[b] Ales Styskalik,[a,c] Damien P. Debecker,[d] P. Hubert Mutin,[b] and Jiri Pinkas[a,c]*

[a] Masaryk University, Faculty of Science, Department of Chemistry, Kotlarska 2, 61137 Brno, Czech Republic
[b] Institut Charles Gerhardt Montpellier, UMR 5253, CNRS-Université de Montpellier-ENSCM, Montpellier Cedex 5 34095, France
[c] Masaryk University, CEITEC MU, Kamenice 5, 62500 Brno, Czech Republic
[d] Institute of Condensed Matter and Nanoscience (IMCN), UCLouvain, Place Louis Pasteur 1, 1348 Louvain-La-Neuve, Belgium

*jpinkas@chemi.muni.cz

NMR spectroscopy

The $^{31}P\{^{1}H\}$ NMR spectra of methyl and tert-butyl phosphonate silylesters show a singlet resonance at 10.5 and 19.7 ppm, respectively. In case of phenyl, bridging phenylene, and brindging biphenylene phosphonate esters, the singlets are shifted to 0 ppm in all cases (Fig S1, S3, S5, S7, S9).

The $^{13}C\{^{1}H\}$ NMR ($CDCl_3$, ppm) of trimethylsilyl-methylphosphonate: δ 13.9 (d, $^{1}J_{PC}$ = 150 Hz, CH_3), δ 0.0 (Me_3Si); trimethylsilyl tert-butylphosphonate: δ 30.8 (d, $^{1}J_{PC}$ = 150 Hz, $C(CH_3)_2$), 24.9 (d, $^{2}J_{PC}$ = 2 Hz, $C(CH_3)_2$), δ 0.0 (Me_3Si). Trimethylsilyl esters of phenyl, bridging phenylene, and brindging biphenylene phosphonates show a resonance at 0 ppm (Me_3Si) and a group of resonances at 125–143 ppm (aromatic rings), Fig. S2,S4, S6, S8, S10.

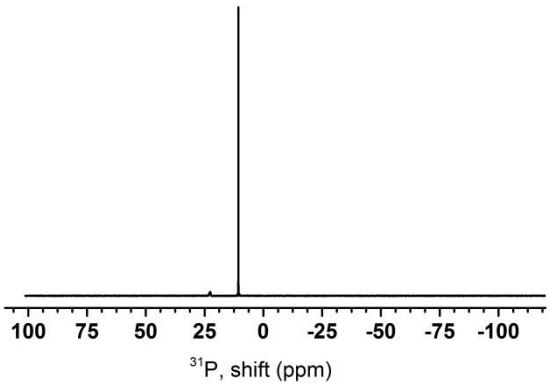

Fig. S1 $^{31}P\{^{1}H\}$ NMR of $MeP(O)(OSiMe_3)_2$ in $CDCl_3$

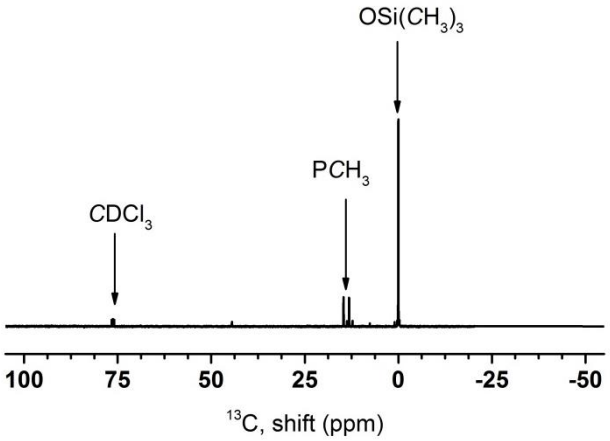

Fig. S2 $^{13}C\{^{1}H\}$ NMR of $MeP(O)(OSiMe_3)_2$ in $CDCl_3$

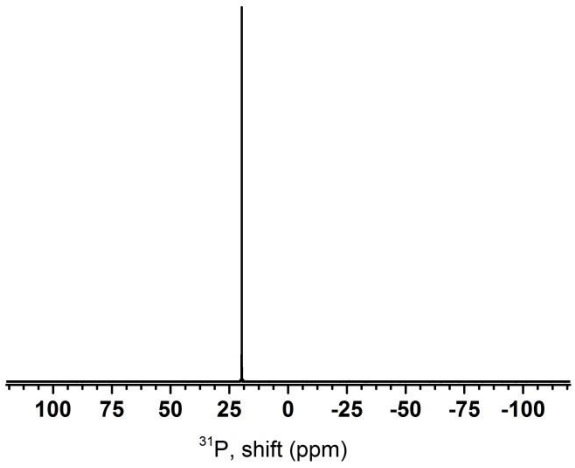

Fig. S3 $^{31}P\{^{1}H\}$ NMR of $^{t}BuP(O)(OSiMe_3)_2$ in $CDCl_3$

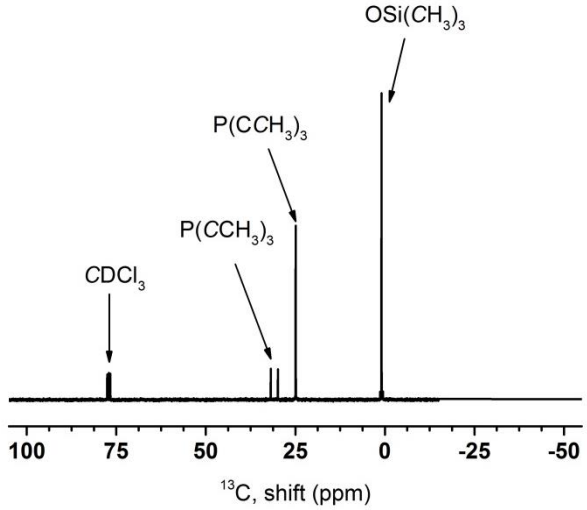

Fig. S4 $^{13}C\{^{1}H\}$ NMR of $^{t}BuP(O)(OSiMe_3)_2$ in $CDCl_3$

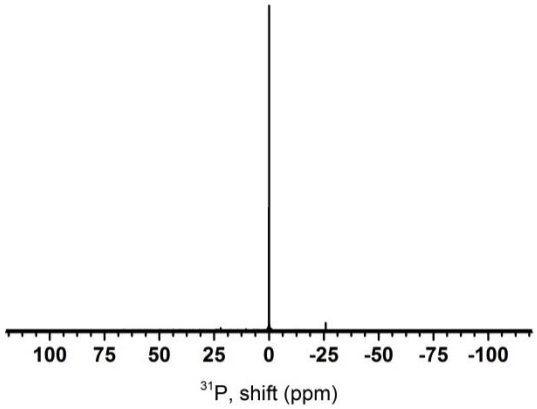

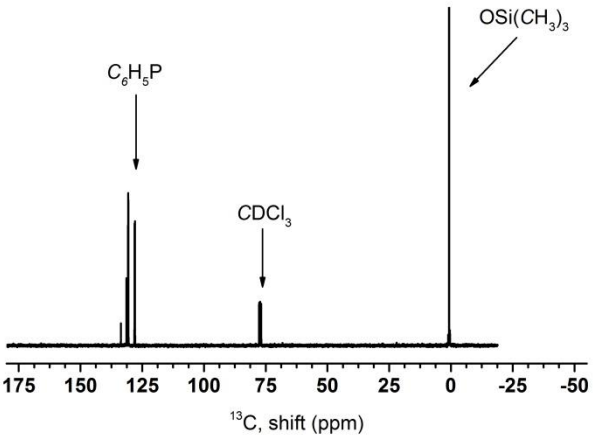

Fig. S6 $^{13}C\{^{1}H\}$ NMR of $PhP(O)(OSiMe_3)_2$ in $CDCl_3$

Fig. S5 $^{31}P\{^{1}H\}$ NMR of $PhP(O)(OSiMe_3)_2$ in $CDCl_3$

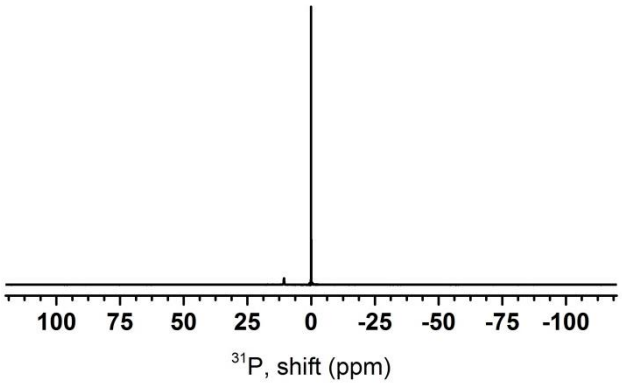

Fig. S7 $^{31}P\{^{1}H\}$ NMR of $[(Me_3SiO)_2P(O)–C_6H_4–P(O)(OSiMe_3)_2]$ in $CDCl_3$

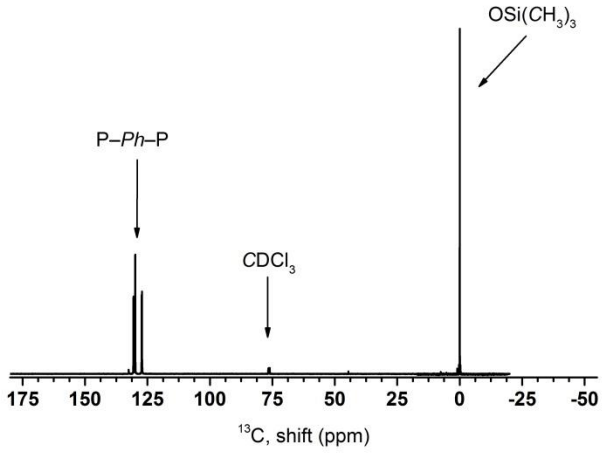

Fig. S8 $^{13}C\{^{1}H\}$ NMR of $(Me_3SiO)_2P(O)–C_6H_4–P(O)(OSiMe_3)_2$ in $CDCl_3$

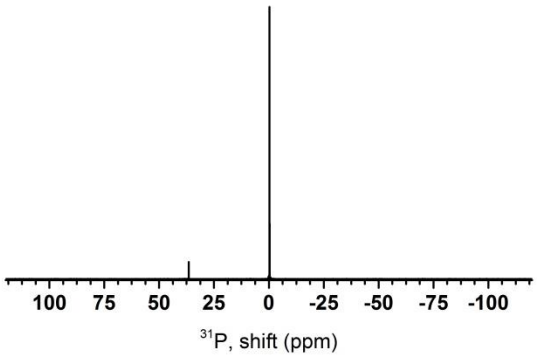

Fig. S9 $^{31}P\{^{1}H\}$ NMR of $[(C_6H_4)P(O)(OSiMe_3)_2]_2$ in $CDCl_3$

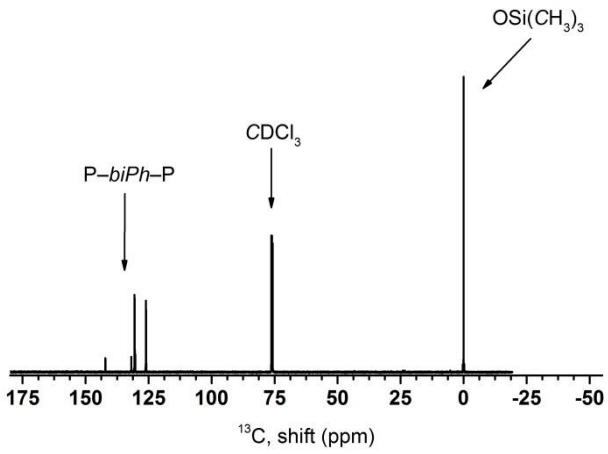

Fig. S10 $^{13}C\{^{1}H\}$ NMR of $[(C_6H_4)P(O)(OSiMe_3)_2]_2$ in $CDCl_3$

Table S1 Precursors amounts and their ratios

Sample	m(Al),[a] g	n(Al),[b] mmol	Al:P nominal	Al:P actual	m(P),[c] g	n(P),[d] mmol
AlP0.8	1.0242	6.43	0.8	0.799	2.5322	8.05
AlP0.9	1.0371	6.51	0.9	0.897	2.2823	7.26
AlP1.0	0.6096	3.83	1.0	0.980	1.2295	3.91
AlP1.1	1.0558	6.63	1.1	1.085	1.9218	6.11
AlP1.4	1.3651	8.57	1.4	1.443	1.8680	5.94
AlP_P[e]	0.6040	3.79	1.0	0.969	1.2309	3.91
AlP_B[f]	0.7740	4.86	1.0	1.011	1.5116	4.81
AlP_F[g]	0.8670	5.44	1.0	0.951	1.8015	5.73
AlP_bPh	0.4552	2.86	0.667	0.671	1.1229	2.13
AlP_bPh2	0.3852	2.42	0.667	0.669	1.0897	1.81
AlP_Me	0.9187	5.77	0.667	0.669	2.0744	8.63
AlP_Ph	0.5335	3.35	0.667	0.669	1.5135	5.00
AlP_Bu	0.6928	4.35	0.667	0.668	1.839	6.51

[a] mass of $Al(NMe_2)_3$, [b] molar amount of $Al(NMe_2)_3$, [c] mass of a phosphorus precursor, [d] molar amount of a phosphorus precursor, mass of templates used: [e] P123 - 0.4668 g, [f] Brij 58 - 0.5091 g, [g] F127 - 0.6816 g

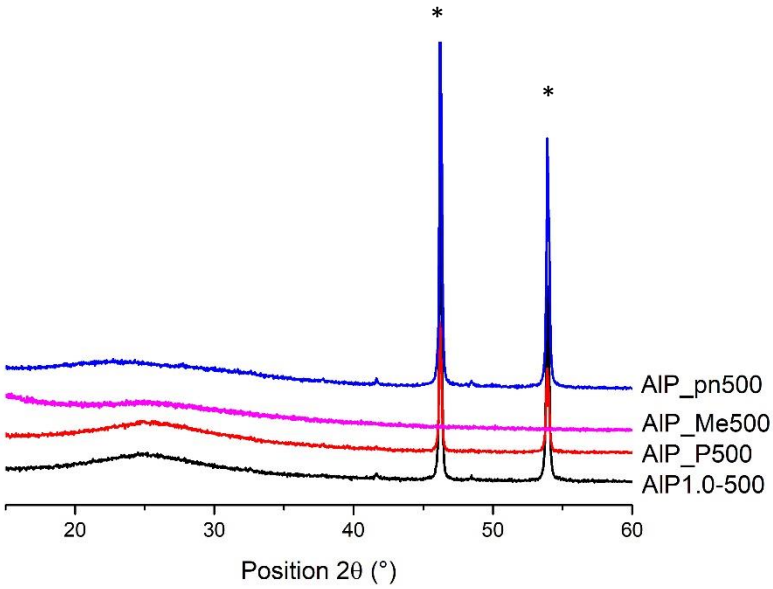

Fig. S11 Powder XRD diffractograms of selected samples (asterisks denote Pt holder diffractions), AlP_Me-500 was measured on a diffraction-free silicon holder

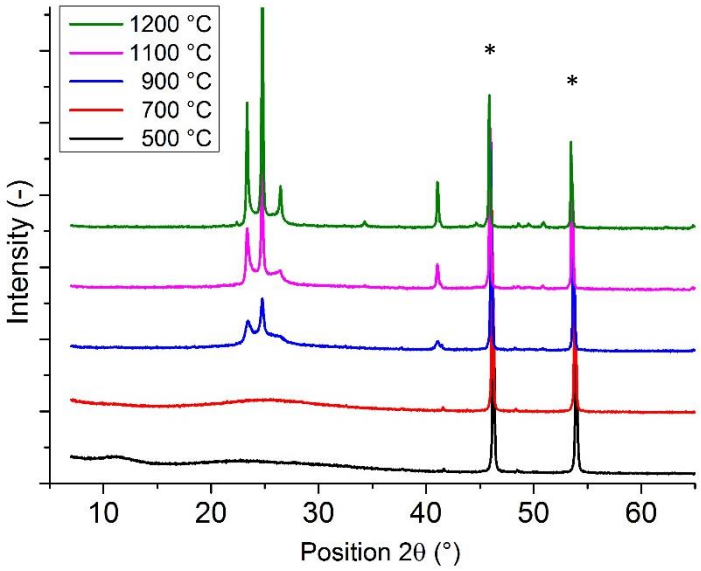

Fig. S12 Powder HT-XRD diffractograms of AlP_pn at different temperatures (asterisks denote Pt holder diffractions)

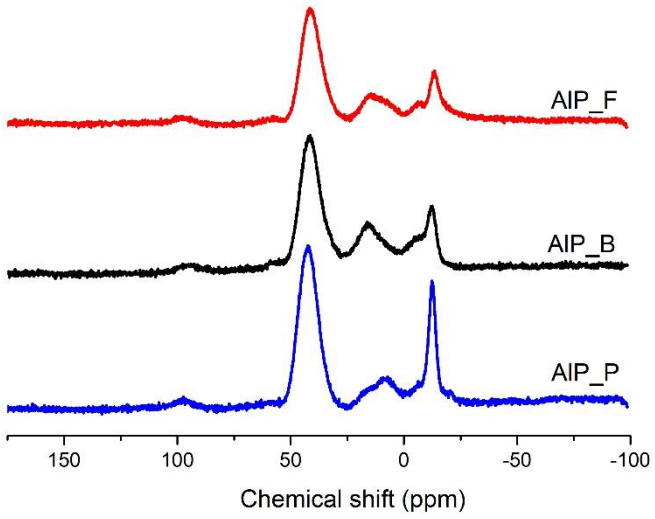

Fig. S13 ^{27}Al MAS NMR of templated phosphate samples

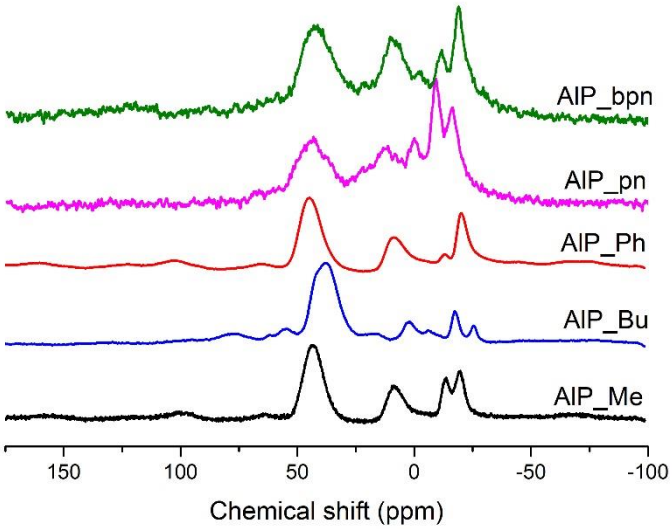

Fig. S14 ^{27}Al MAS NMR of phosphonate and bridging phosphonate samples

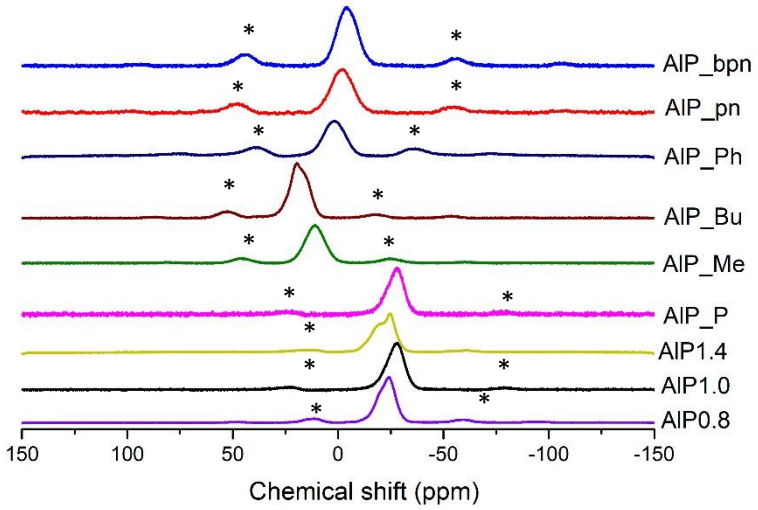

Fig. S15 ^{31}P MAS NMR of xerogels (asterisks denote spinning side bands)

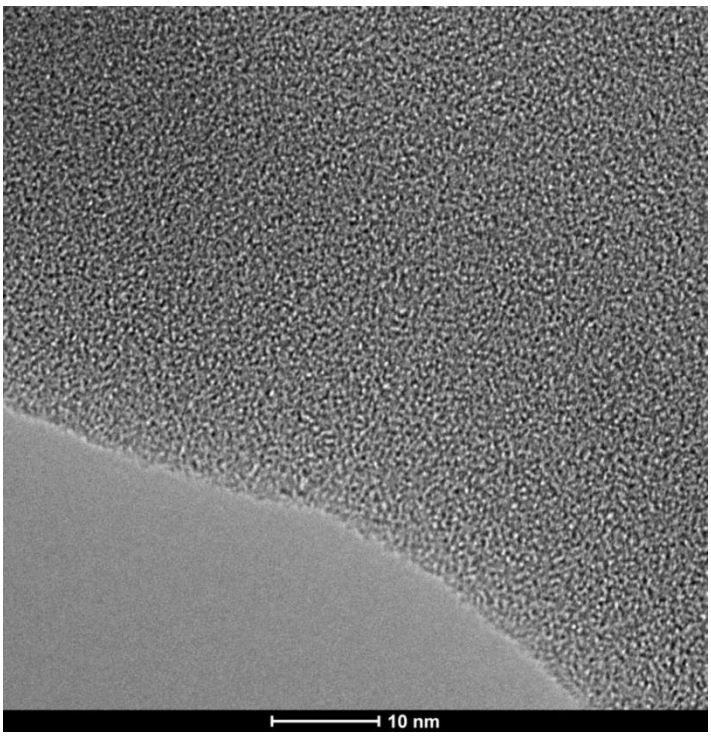

Fig. S16 TEM image of AlP1.0 sample

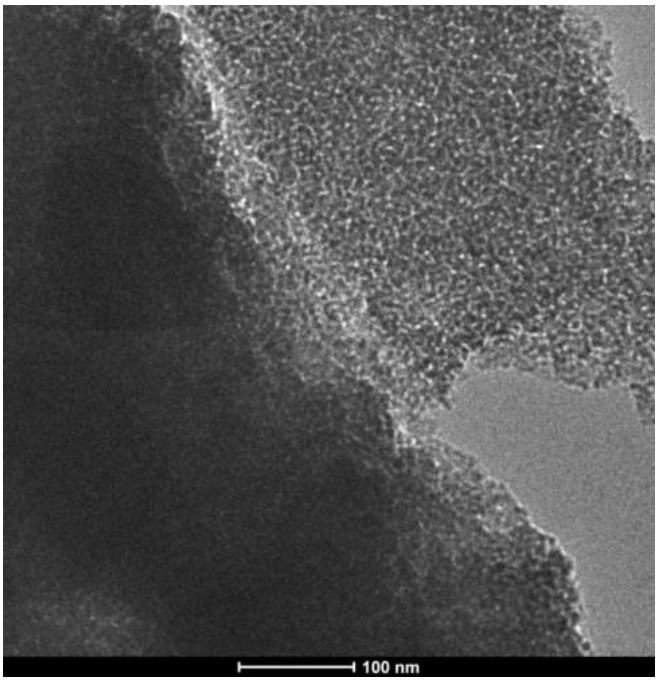

Fig. S17 TEM image of AlP_pn sample

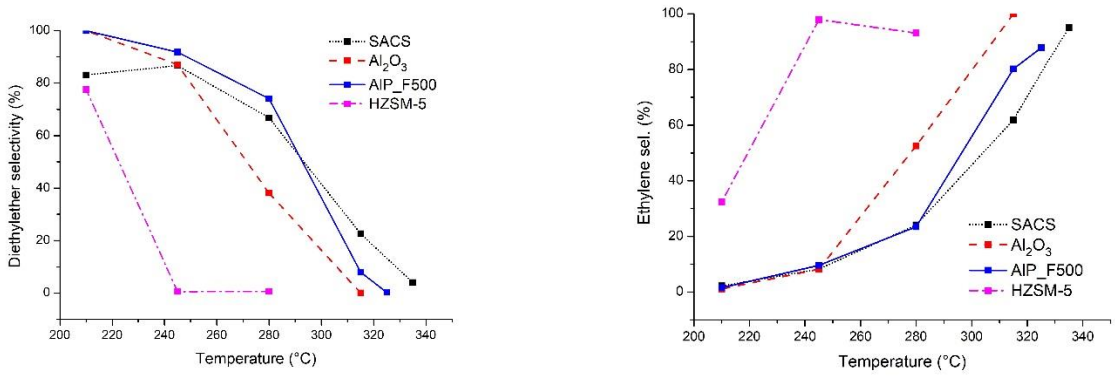

Fig. S18 Selectivity to diethylether (left) and to ethylene (right) for AlP_F500 and three commercial benchmarks